NGU
Norges geologiske undersøkelse
Geological Survey of Norway

GEOLOGI FOR SAMFUNNET
GEOLOGY FOR SOCIETY

NGU Report 2014.011

Assessment of quartz qualities XV

NGU
Norges geologiske undersøkelse
Geological Survey of Norway

Geological Survey of Norway
NO-7441 Trondheim, Norway
Tel.: 47 73 90 40 00
Telefax 47 73 92 16 20

REPORT

Report no.: 2014.011 | ISSN 0800-3416 | Grading: Confidential until 15.03.2016

Title:
Assessment of quartz qualities XV

Authors:
Axel Müller, Jan Egil Wanvik

Client:
Daniel Smith, Atherton Minerals Exploration Pty Ltd

County:
Queensland, Australia

Commune:
Georgetown

Map-sheet name (M=1:250.000)
Georgetown

Map-sheet no. and -name (M=1:50.000)
Not specified

Deposit name and grid-reference:
Lighthouse & Midway, Mt. Talbot, Blow 2

Number of pages: 31 Price (NOK): 160,00
Map enclosures: -

Fieldwork carried out: -

Date of report: 15.03.2014

Project no.: 343300

Person responsible: Henrik Schiellerup

Summary

The Geological Survey of Norway (NGU) was contacted by Daniel Smith, Atherton Minerals Exploration Pty ltd, Australia, in November 2013 in order to characterize the chemical quality of quartz samples from the Lighthouse & Midway, Mt. Talbot and Blow 2 localities in the Georgetown region in north Queensland, Australia.
The micro inclusion inventory of quartz samples was examined by optical and scanning electron microscopy. Concentrations of structurally bound (lattice-bound) trace elements were analyzed by laser ablation inductively coupled plasma mass spectrometry (LA-ICP-MS). Because lattice-bound trace elements cannot be removed by processing, the determined concentrations correspond to the lowest concentrations (best chemical quality) which may be achieved if the most modern and advanced quartz processing techniques are applied.

Quartz from *Mt. Talbot* contains mineral micro inclusions of muscovite ($KAl_2(AlSi_3O_{10})(OH)_2$), K-feldspar ($(K,Na)AlSi_3O_8$), biotite, ($K(Fe,Mg)Al(Al_2Si_2O_{10})(OH)_2$), rutile ($TiO_2$), and magnetite ($Fe_2O_3$). Liquid-rich fluid inclusions (0.1 to 10 µm) are very common which represent significant Na and K contaminants. The Mt. Talbot quartz has low total trace element contents of 38 to 58 ppm, without considering Ca, Na, and K due to the high detection limits. Elevated K, Ti, and Fe concentrations are caused by micro inclusions of biotite (K, Fe) and rutile (Ti). The product will be highly suitable for solar-grade silicon production, even if only simple processing will be applied. By applying advanced processing technology the quartz can possibly be used for optical glass production.

Quartz from *Lighthouse & Midway* is very rich in fluid inclusions which represent significant Na and K contaminants. In addition, calcite ($CaCO_3$) micro inclusions are common which are responsible for the partially high Ca concentrations (<5 to 63 ppm). Quartz from these localities has variable total trace element concentrations between 28 and 127 ppm. Due to the variable and partially moderately high content of structurally incorporated Al and the high abundance of fluid inclusions, a possible processed quartz product will ideally fulfil the requirements for intermediary quality. The quality is sufficient to use the quartz as raw material for solar-grade silicon production due to relatively low B and P concentrations.

The megacrystic quartz from *Blow 2* (sample 26) shows a high abundance of fluid inclusions being significant Na and K contaminants. The quartz contains pyrite (FeS_2) and chalcopyrite ($CuFeS_2$) micro inclusions which are significant Fe contaminants. Quartz from Blow 2 has high Li, Al, Fe, and K and very high Ti. The total content of the analysed structurally incorporated trace elements is 163 and 196 ppm. A processed quartz product will ideally fulfil the requirements of intermediary quality which may be suitable for solar-grade silicon production.

Keywords: Technical report	quartz	Queensland
LA-ICP-MS		

Content

Figures

Tables

1. Introduction

The Geological Survey of Norway (NGU) was contacted by Daniel Smith, Atherton Minerals Exploration Pty ltd, Australia, in November 2013 in order to characterize the chemical quality of quartz samples from the Lighthouse & Midway, Mt. Talbot and Blow 2 localities in the Georgetown region in north Queensland, Australia. Previous studies and tests carried out on the same deposits showed that the quartz has high quality containing 99.95 to 99.99 % SiO_2.

Seven quartz samples were send to the Geological Survey of Norway in November 2013. Four methods were applied: (1) optical microscopy to characterize the type and abundance of fluid and mineral micro inclusions (>2 µm) in quartz crystals, (2) scanning electron microscopy (SEM) to determine the chemistry of mineral micro inclusions, (3) scanning electron microscope cathodoluminescence (SEM-CL) imaging to examine the luminescence characteristics of quartz, and (4) laser ablation inductively coupled plasma mass spectrometry (LA-ICP-MS) to analyze the concentrations of crystallographic bound (lattice-bound) trace elements (Al, Ti, Li, P, B, Fe, K, Na, Ca, Ge, Mn, Be) in single quartz crystals. All four methods were carried out on petrological thick sections (ca. 20 × 30 × 0.3 mm) mounted on standard glass slides (2.8 × 4.8 × 0.2 cm). The analytical results are discussed with respect to the potential chemical quality of possible quartz products produced from the investigated quartz samples.

2. Samples and methods

2.1 Samples

Seven quartz samples were send to the Geological Survey of Norway in November 2013. The macroscopic appearance of the samples is photographically documented in Figures 1 and 2. The macroscopic features of the samples are given in Table 1.

Figure 1. *Photographs of quartz samples 21 to 24 as they were sent to NGU.*

Figure 2. *Photographs of quartz samples 25 to 27 as they were sent to NGU.*

Table 1. *Macroscopic features of quartz samples. The crystal size were determined by using optical microscopy (see chapter 3.1).*

sample	locality	colour	transparency	crystal size	other characteristic features	macroscopic impurities
21	Mt Talbot	snow white	milky opaque	0.03-0.8 mm	sugar-grained texture	minor iron oxide staining at open fractures
22	Lighthouse & Midway	snow white	milky opaque	0.01-0.2 mm	greasy lustre of fresh fracture plains	minor iron oxide staining within crystals
23	Lighthouse & Midway	snow white	milky opaque	0.01 mm - 5 cm	greasy lustre of fresh fracture plains	minor iron oxide staining within crystals
24	Lighthouse & Midway	snow white	milky opaque	0.01 mm - 5 cm	greasy lustre of fresh fracture plains	minor iron oxide staining within crystals
25	Mt Talbot	snow white	milky opaque	0.03-0.8 mm	sugar-grained texture	-
26	Blow 2	greyish white	semi-opaque	>5 cm	large, intergrown pegmatitic crystals	-
27	Lighthouse & Midway	snow white	milky opaque	0.01 mm - 5 cm	greasy lustre of fresh fracture plains	minor iron oxide staining within crystals

2.2 Sample preparation

Petrological thick sections were prepared at the Dettmar Dissection Technology GmbH & Co. KG in Bochum, Germany for microscopic investigations (optical microscopy and scanning electron microscopy) and quartz analysis (laser ablation inductively coupled plasma mass spectrometry). Petrological sections are surface-polished rock slabs (ca. 20 × 30 × 0.3 mm), in this case quartz slabs, with a thickness of 300 µm mounted with Epoxy on a 4.8 × 2.8 × 0.2 cm large glass slide.

2.3 Optical microscopy

The sections were examined with a petrological microscope type Zeiss Axioplan 2 in order to document the frequency and type of fluid and mineral micro inclusions >2 µm. Microphotographs were taken with an AxioCam digital camera attached to the microscope using magnifications from 250 to 1000×. The camera was run by the software AxioVision 4.7. Photograph scaling and processing were performed with the same software.

2.4 Scanning electron microscopy

Scanning electron microscopy (SEM) was applied to document the micro inclusion inventory of quartz by backscattered electron (BSE) imaging and to determine the semi-quantitative composition of micro inclusions in quartz crystals. The SEM investigations were carried out on carbon-coated tick sections using the LEO 1450VP analytical SEM with an attached INCA EDS detector from Oxford Instruments. The applied acceleration voltage and current at the sample surface were 20 kV and ~2 nA, respectively. BSE images were collected from one scan of 43 s photo speed and a processing resolution of 1,024 x 768 pixels and 256 grey levels. Semi-quantitative analysis in micro inclusions were performed with the EDS detector and processed with INCAEnergy software.

2.5 Scanning electron microscope cathodoluminescence

Scanning electron microscope cathodoluminescence (SEM-CL) images were obtained with a Centaurus BS Bialkali CL detector attached to the LEO 1450VP analytical SEM. The applied voltage and current were the same as for the SEM investigations. The Bialkali tube has a CL response range from 300 (violet) to 650 nm (red). The detector sensitivity peaks in the violet spectrum range around 400 nm. SEM-CL images were collected from one scan of 43 s photo speed and a processing resolution of 1,024 x 768 pixels and 256 grey levels.

SEM-CL imaging reveals micro-scale (<1 mm) growth zoning, alteration structures and different quartz generations which are not visible with other methods. Grey-scale contrasts are caused by the heterogeneous distribution of lattice defects (e.g., oxygen and silicon vacancies, broken bonds) and lattice-bound trace elements (e.g., Götze et al. 2001). Although the physical background of the quartz CL is not fully understood, the structures revealed by CL give information about crystallization, deformation and fluid-driven overprint.

2.6 Laser ablation inductively coupled plasma mass spectrometry

Concentrations of Li, Be, B, Al, P, Ti, Ca, Na, K, Mn, Fe, and Ge were analyzed in situ by laser-ablation inductively-coupled plasma mass spectrometry (LA-ICP-MS). The analyses were performed on the double-focusing sector field mass spectrometer model ELEMENT XR ICP-MS with an attached New Wave UP193FX Excimer 193-nm laser probe. The laser had a repetition rate of 15 Hz, a speed of 15 µm s^{-1}, a spot size of 75 µm, and energy fluence of about 14 mJ cm^{-2} on the sample surface. Raster ablation was applied in the centre of quartz crystals on an area of approximately 250 x 500 µm (Figure 3). The approximate depth of ablation was between 40 and 100 µm depending on the crystallographic orientation and absorption behaviour of the individual quartz crystals.

A Hitachi CCD video camera type KP-D20BU attached to the laser system facilitates the observation of the laser ablation process to avoid the analysis of micro mineral and fluid inclusions (>0.1 µm) occurring in the natural quartz crystals to be analyzed. In the case no inclusions are hit by the laser, the determined trace element concentrations correspond to the contents of ions which are structurally bound in the quartz lattice. Because lattice-bound trace elements cannot be removed by processing, these concentrations correspond to the lowest concentrations which may be achieved if the most modern and advanced quartz processing techniques are applied including floatation, magnetic separation, and acid leaching of ground quartz sand. It is important to note that the determined trace element concentrations will not correspond to the trace element concentrations of an unprocessed quartz product. Quartz grains analyzed in the frame of this project are very rich in fluid inclusions and contain some mineral inclusions (see chapters below) and, therefore, concentrations of elements occurring in these inclusions, predominantly Na, K, Ca, and Fe, are superimposed on the concentrations of lattice-bound elements.

The carrier gas for transport of the ablated material to the ICP-MS was He mixed with Ar. External calibration was performed using four silicate glass reference materials (NIST SRM 610, 612, 614, 616), the NIST SRM 1830 soda-lime float glass, the BAM No.1 amorphous SiO_2 glass and the synthetic pure quartz monocrystal Qz-Tu. Certified, recommended and proposed values for these reference materials were taken from the certificates of analysis where available, or otherwise from the web site Geological and Environmental Reference Materials (GeoReM 2014). The isotope ^{29}Si was used as the internal standard. A linear regression model, including several measurements of the different reference materials, was used to define the calibration curve for each element. For the calculation of P concentrations, the procedure of Müller et al. (2008) was applied. Ten sequential measurements on the ‘‘SiO_2 blank’’ crystal were used to estimate the limits of detection (LOD) which were based on 3x standard deviation (3σ) of the ten measurements. LODs vary for each analysis sequence (measurement day). Examples of LODs are given in Table 3. The analytical error ranges within 10% of the absolute concentration of the element. Detection limits for the alkali metals Na, K, and Ca are relatively high compared to other elements because they are difficult to measure with the LA-ICP-MS system. More details of the measurement procedure are provided by Flem et al. (2002) and Flem and Müller (2012).

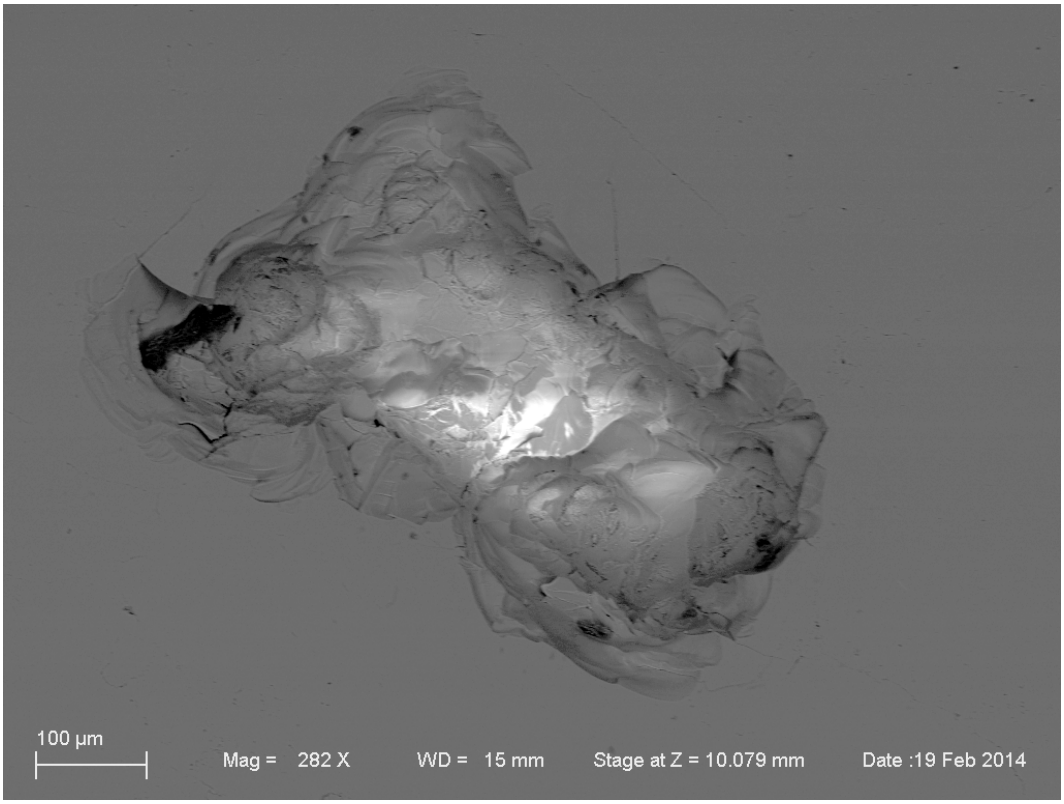

Figure 3. *Backscattered electron image showing an example of a laser ablation crater in quartz after analyses. Sample 25, analysis 25-A.*

3. Results

3.1 Quartz mineralogy and micro inclusion inventory

3.1.1 Sample 21, Mt. Talbot

The mosaic-like, recrystallized quartz crystal texture consists of small crystals ranging in size from 30 to 800 µm with an average of about 250 µm (Figure 4). Small (0.1 to 10 µm) liquid-rich fluid inclusions[1] are very common and are responsible for the macroscopically opaque appearance of quartz. They typically occur at grain boundaries of recrystallized grains and in crosscutting trails representing healed micro fractures. The properties of the fluid inclusions indicate a moderate salinity of the fluid with 3 to 8 vol.% NaCl(+KCl). Several types mineral inclusions were identified in quartz sample 21 (in order of frequency): K-feldspar ($(K,Na)AlSi_3O_8$; 40 to 400 µm), biotite ($K(Fe,Mg)Al(Al_2Si_2O_{10})(OH)_2$; 15 to 100 µm) and magnetite (Fe_2O_3; 10 to 40 µm; Figures 5A-C). The quartz shows dull cathodoluminescence with different shades (Figure 6A). The almost non-luminescent quartz (black in the SEM-CL image in Figure 6A) represent domains of newly crystallized quartz to due recrystallization and deformation.

3.1.2 Sample 22, Lighthouse & Midway

The strongly recrystallized quartz crystal texture consists of small crystals ranging in size from 10 to 200 µm with an average of about 80 µm (Figure 7). Small (0.1 to 40 µm) liquid- and vapor-rich fluid inclusions are very common and are responsible for the macroscopically opaque appearance of quartz (Figure 7D). They occur within crystals, along healed micro fractures and along grain boundaries. The properties of fluid inclusions indicate high salinities of the fluids with 5 to 15 wt% NaCl(+KCl). The only type of mineral inclusions which could be detected are tiny (8 to 25 µm) calcite inclusions ($CaCO_3$; Figure 5D). The dull luminescent images of quartz document a strong secondary alteration and penetration by hydrothermal fluids (Figure 6B).

3.1.3 Sample 23, Lighthouse & Midway

The partially recrystallized quartz crystal texture consists of relative large crystals (2 to 5 cm) crosscut by recrystallized vein-like micro structures with crystal sizes ranging from 10 to 100 µm (Figure 8). Small (0.1 to 40 µm) liquid- and vapor-rich fluid inclusions are very common and are responsible for the macroscopically opaque appearance of quartz. They follow commonly healed micro fractures. The properties of fluid inclusions indicate high salinities of the fluids with 5 to 15 wt% NaCl(+KCl). The only type of mineral inclusions which could be detected are tiny (8 to 25 µm) calcite inclusions ($CaCO_3$; Figure 5D) similar to sample 22. The dull luminescent images of quartz document a strong secondary alteration and penetration by hydrothermal fluids (Figure 6C) similar to sample 22.

3.1.4 Sample 24, Lighthouse & Midway

The partially recrystallized quartz crystal texture consists of relative large crystals (2 to 5 cm) crosscut by recrystallized vein-like micro structures with crystal sizes ranging from 10 to 100

[1] Fluid inclusions are tiny quantities of liquid and/or vapor trapped as impurities within minerals like quartz. Their sizes range from submicroscopic up to several hundred micrometers in diameter. The liquids and gases were either trapped during initial mineral growth (primary fluid inclusions) or after primary crystallization when fluids moved through the rock along micro fractures and fluids were trapped during the healing of these fractures (secondary fluid inclusions).

µm (Figure 9). Small (0.1 to 40 µm) liquid- and vapor-rich fluid inclusions are very common and are responsible for the macroscopically opaque appearance of quartz. They occur within crystals, along healed micro fractures and along grain boundaries. The properties of fluid inclusions indicate high salinities of the fluids with 5 to 15 wt% NaCl(+KCl). Micro inclusions of muscovite ($KAl_2(AlSi_3O_{10})(OH)_2$; 5 to 40 µm; Figure 5E) and calcite ($CaCO_3$; 5 µm) were identified. The dull luminescent images of quartz document a strong secondary alteration and penetration by hydrothermal fluids (Figure 6D) similar to samples 22 and 23.

3.1.5 Sample 25, Mt. Talbot

The mosaic-like, recrystallized quartz crystal texture consists of small crystals ranging in size from 30 to 800 µm with an average of about 250 µm (Figure 10). Small (0.1 to 10 µm) liquid-rich fluid inclusions are very common and are responsible for the macroscopically opaque appearance of quartz. They typically occur at grain boundaries of recrystallized grains and in crosscutting trails representing healed micro fractures. The properties of the fluid inclusions indicate a moderate salinity of the fluid with 3 to 8 vol.% NaCl(+KCl). Three types of mineral inclusions were identified in quartz sample 25 (in order of frequency): muscovite ($KAl_2(AlSi_3O_{10})(OH)_2$; 10 to 30 µm; Figure 5F), biotite ($K(Fe,Mg)Al(Al_2Si_2O_{10})(OH)_2$; 10 to 20 µm), and rutile (TiO_2; 8 µm; Figure 11A). The quartz shows dull cathodoluminescence with different shades (Figure 12A). The almost non-luminescent quartz (black in the SEM-CL image in Figure 12A) represent domains of newly crystallized quartz to due recrystallization and deformation.

3.1.6 Sample 26, Blow 2

Sample 26 consists of large, pegmatitic quartz crystals with sizes of at least 5cm (Figure 13). Small (0.1 to 40 µm) liquid-rich fluid inclusions are common but less abundant compared to the other investigated quartz samples. The inclusions occur along trails following healed micro fractures. The properties of the fluid inclusions indicate a moderate salinity of the fluid with 3 to 8 vol.% NaCl(+KCl). Two types of mineral inclusions were identified in quartz sample 26 (in order of frequency): pyrite (FeS_2; 5-20 µm; Figure 11C, D) and chalcopyrite ($CuFeS_2$; 8 µm; Figure 11B). Quartz of sample 26 shows a bright luminescence which is very different to all other investigated samples. The bright CL indicates a high content of lattice-bound Ti (Müller et al. 2002). The bright luminescent quartz is superimposed by a secondary non-luminescent quartz generation healing micro fractures and domains around fluid inclusions (Figure 12B).

3.1.7 Sample 27, Lighthouse & Midway

The partially recrystallized quartz crystal texture consists of relative large, slightly deformed crystals (2 to 5 cm) crosscut by recrystallized vein-like structures with crystal sizes ranging 10 to 100 µm (Figure 14). Small (0.1 to 40 µm) liquid- and vapor-rich fluid inclusions are very common and are responsible for the macroscopically opaque appearance of quartz. They occur within crystals, along healed micro fractures and along grain boundaries (Figure 14D). The properties of fluid inclusions indicate high salinities of the fluids with 5 to 15 wt% NaCl(+KCl). The only type of mineral inclusions detected are tiny (5 to 30 µm) calcite ($CaCO_3$) inclusions similar to those in samples 22, 23, and 24. The dull luminescent images of quartz document a strong secondary alteration and penetration by hydrothermal fluids (Figure 12C) similar to samples 22, 23, and 24.

Table 2. *Micro inclusion inventory of investigated quartz samples.*

sample	**21**	**22**	**23**	**24**	**25**	**26**	**27**
inclusion type	Mt Talbot	Lighthouse & Midway	Lighthouse & Midway	Lighthouse & Midway	Mt Talbot	Blow 2	Lighthouse & Midway
fluid inclusion	very common	very common	very common	very common	very common	very common	very common
	(0.1-10 µm)	(0.1-40 µm)	(0.1-40 µm)	(0.1-40 µm)	(0.1-10 µm)	(0.1-40 µm)	(0.1-40 µm)
magnetite	rare						
Fe_2O_3	(10-40 µm)	-	-	-	-	-	-
biotite	rare				rare		
$K(Mg,Fe)_3AlSi_3O_{10}(F,OH)_2$	(15-100 µm)	-	-	-	(10-20 µm)		-
K-feldspar	rare						
$KAlSi_3O_8$	(40-400 µm)	-	-	-	-		-
muscovite				rare	rare		
$KAl_2(AlSi_3O_{10})(F,OH)_2$	-	-	-	(5-40 µm)	(10-30 µm)		-
rutile					very rare		
TiO_2	-	-	-	-	(8 µm)		-
calcite		rare	rare	very rare			rare
$CaCO_3$	-	(5-20 µm)	(5-10 µm)	(5 µm)-	-		(5-30 µm)
pyrite						rare	
FeS_2	-	-	-	-	-	(5-20 µm)	-
chalcopyrite						very rare	
$CuFeS_2$	-	-	-	-	-	(8 µm)	-

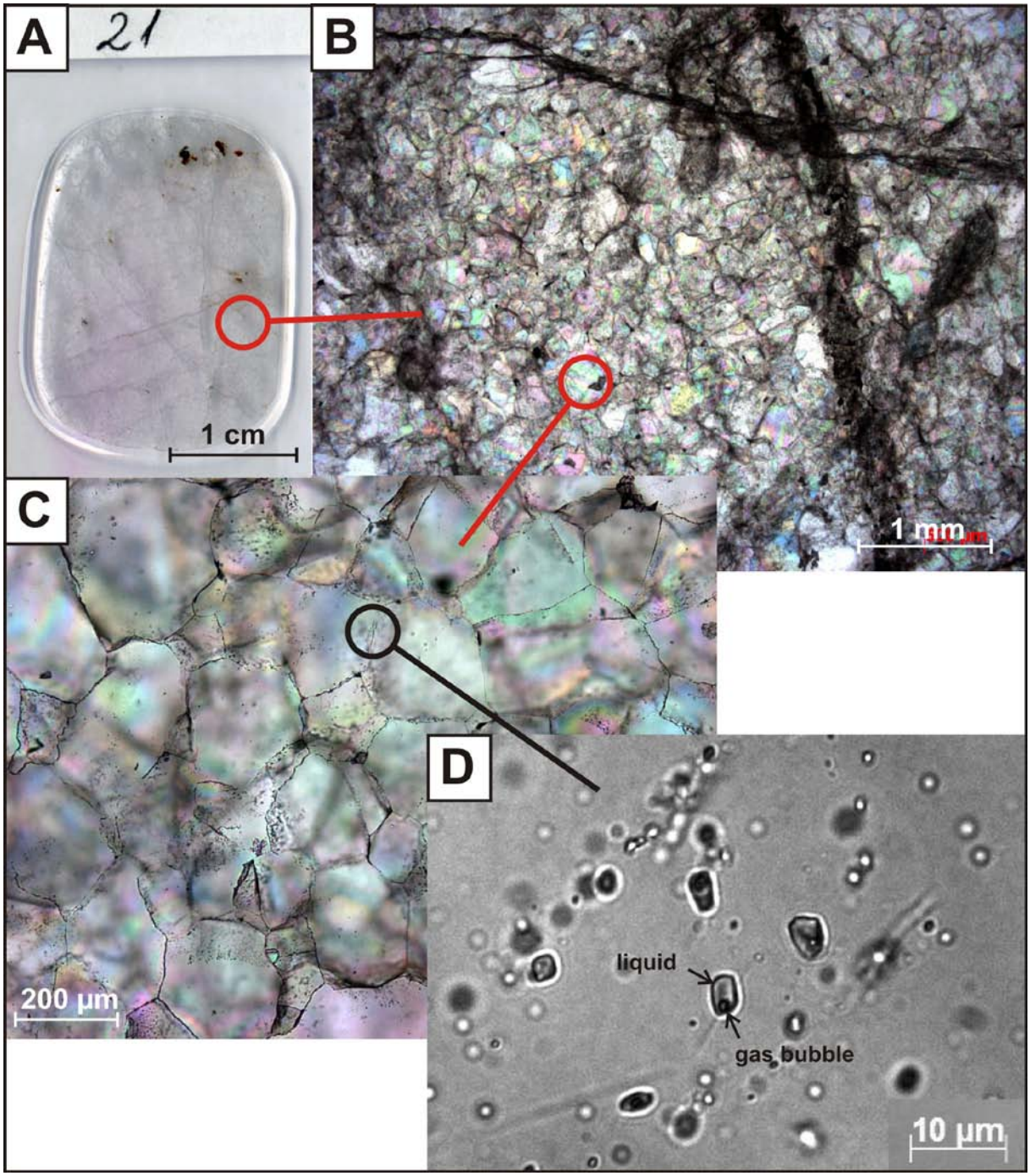

Figure 4. *Microphotographs of quartz sample 21. A – Petrological thick section. B – Optical microscope image (plane light) of quartz showing a high abundance of fluid inclusions causing brownish-black domains (opaqueness) along healed cracks and grain boundaries. C – Microscopic detail showing the mosaic-like texture of quartz texture. The tiny black dots marking the grain boundaries are fluid inclusions. D – Typical liquid rich fluid inclusions containing small gas bubbles.*

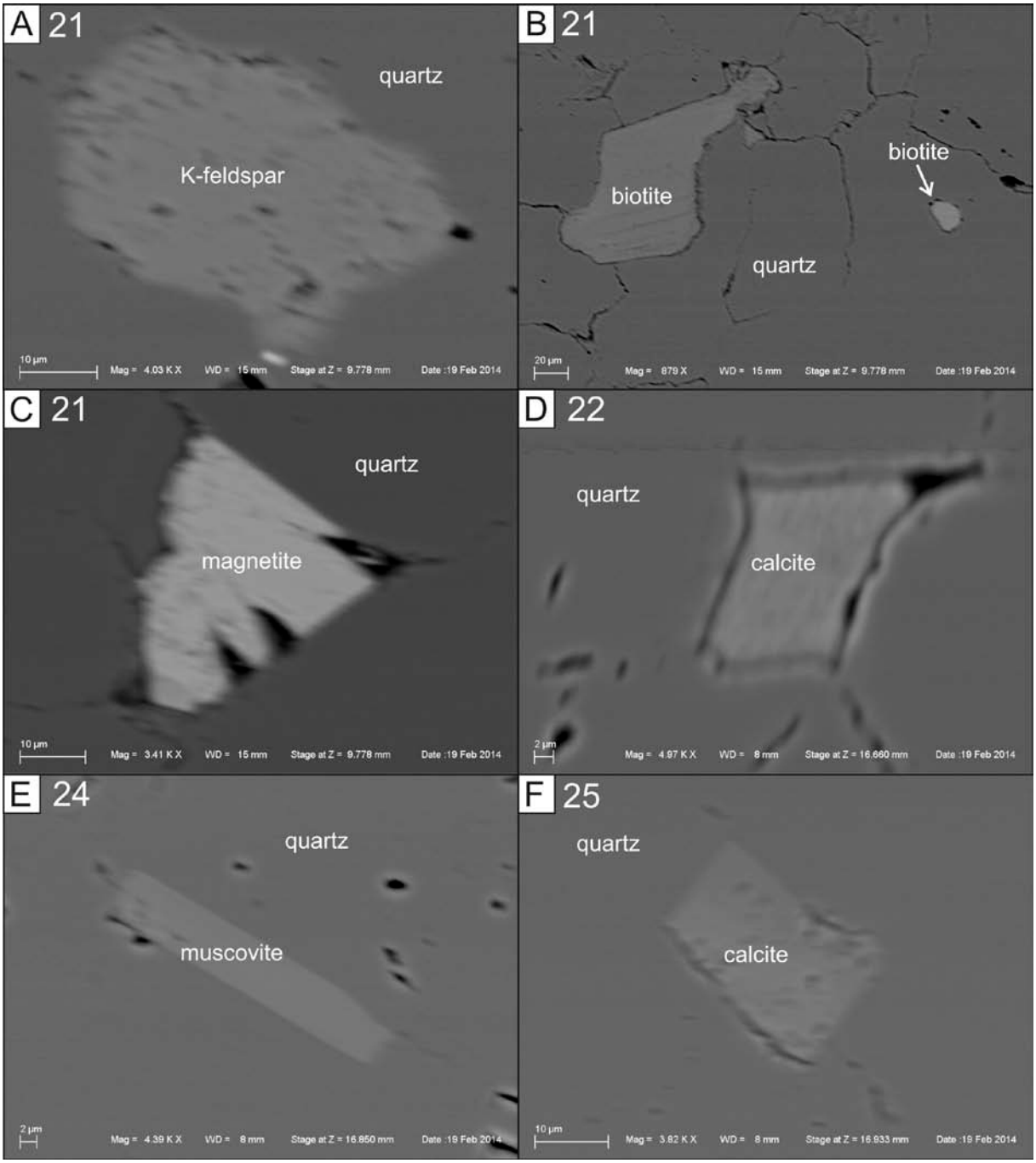

Figure 5. *Backscattered electron images (BSE) of mineral micro inclusions in quartz. A – 50-µm large K-feldspar micro inclusion in sample 21. B – Two biotite micro inclusions (140 and 15 µm) in sample 21. C – 40-µm large magnetite micro inclusion in sample 21. D – 25-µm large calcite micro inclusion in sample 22. E – 35-µm large muscovite micro inclusion in sample 24. F – 28-µm large muscovite micro inclusion in sample 25.*

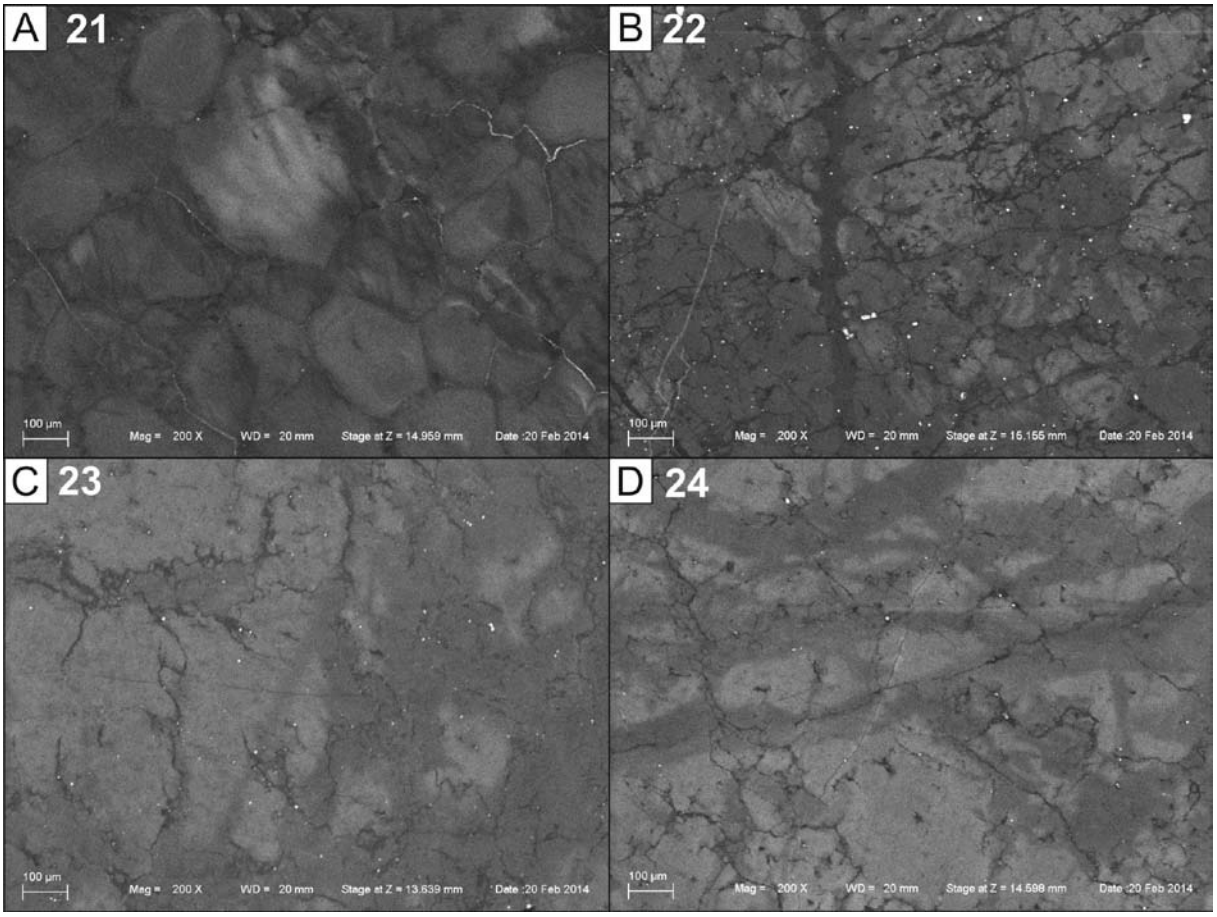

Figure 6. *Scanning electron microscope cathodoluminescence (SEM-CL) images of quartz. A – Dull luminescent quartz of sample 21. The almost black areas represent domains of newly crystallized quartz formed by recrystallization and deformation. B – Dull luminescent quartz of sample 22 with different generations of quartz-healed micro fractures. The small bright luminescent dots (<1 µm) represent presumably calcite inclusions. C – Dull luminescent quartz of sample 23 with different generations of quartz-healed micro fractures. The small bright luminescent dots (<1 µm) represent presumably calcite inclusions. D – Dull luminescent quartz of sample 24 with different generations of quartz-healed micro fractures. The small bright luminescent dots (<1 µm) represent presumably calcite inclusions.*

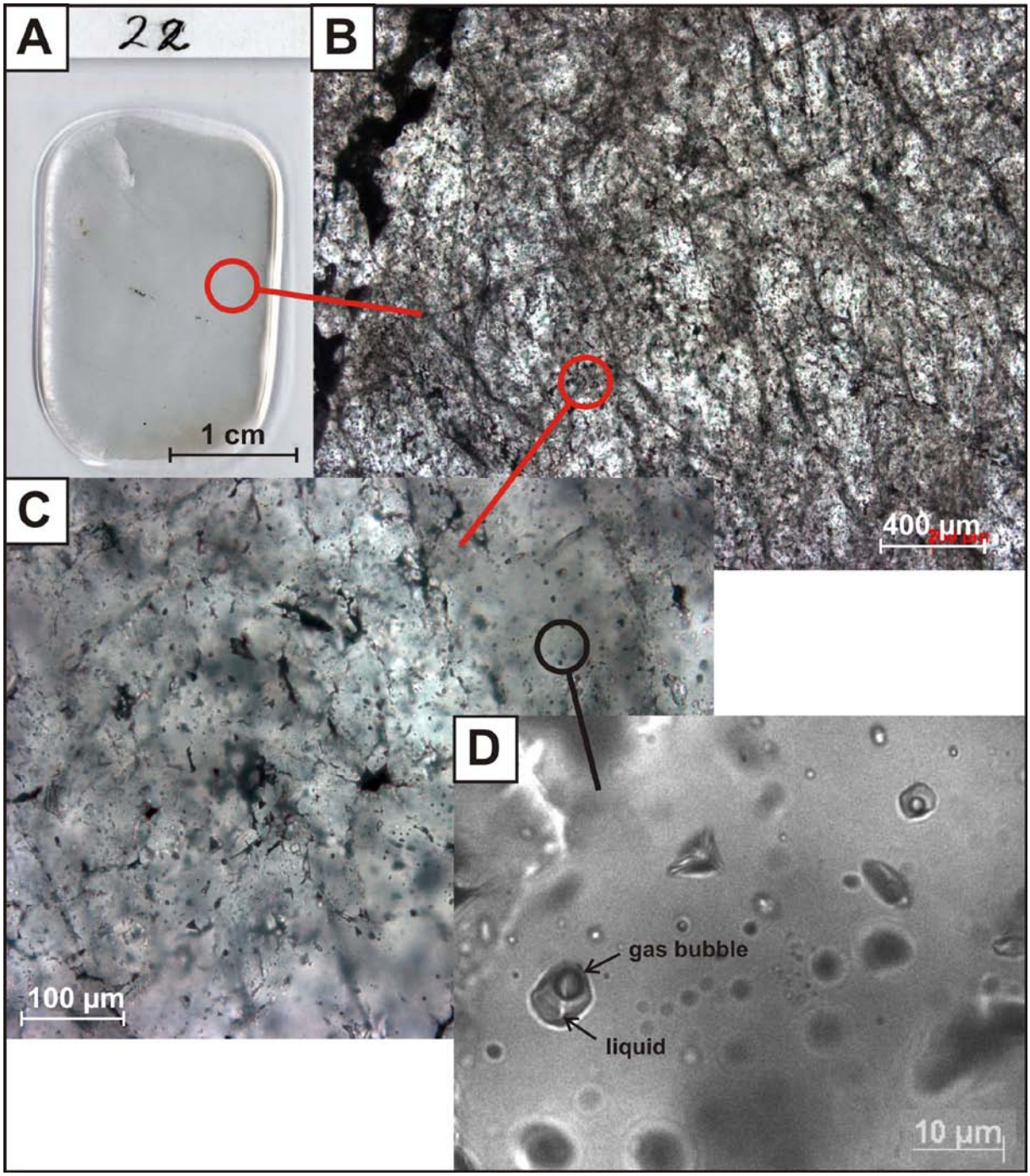

Figure 7. *Microphotographs of quartz sample 22. A – Petrological thick section. B – Optical microscope image (plane light) of quartz showing a high abundance of fluid inclusions causing brownish-black domains (opaqueness). C – Microscopic detail showing the very high abundance of fluid inclusions (black dots/domains). D – Typical liquid rich fluid inclusions containing large gas bubbles.*

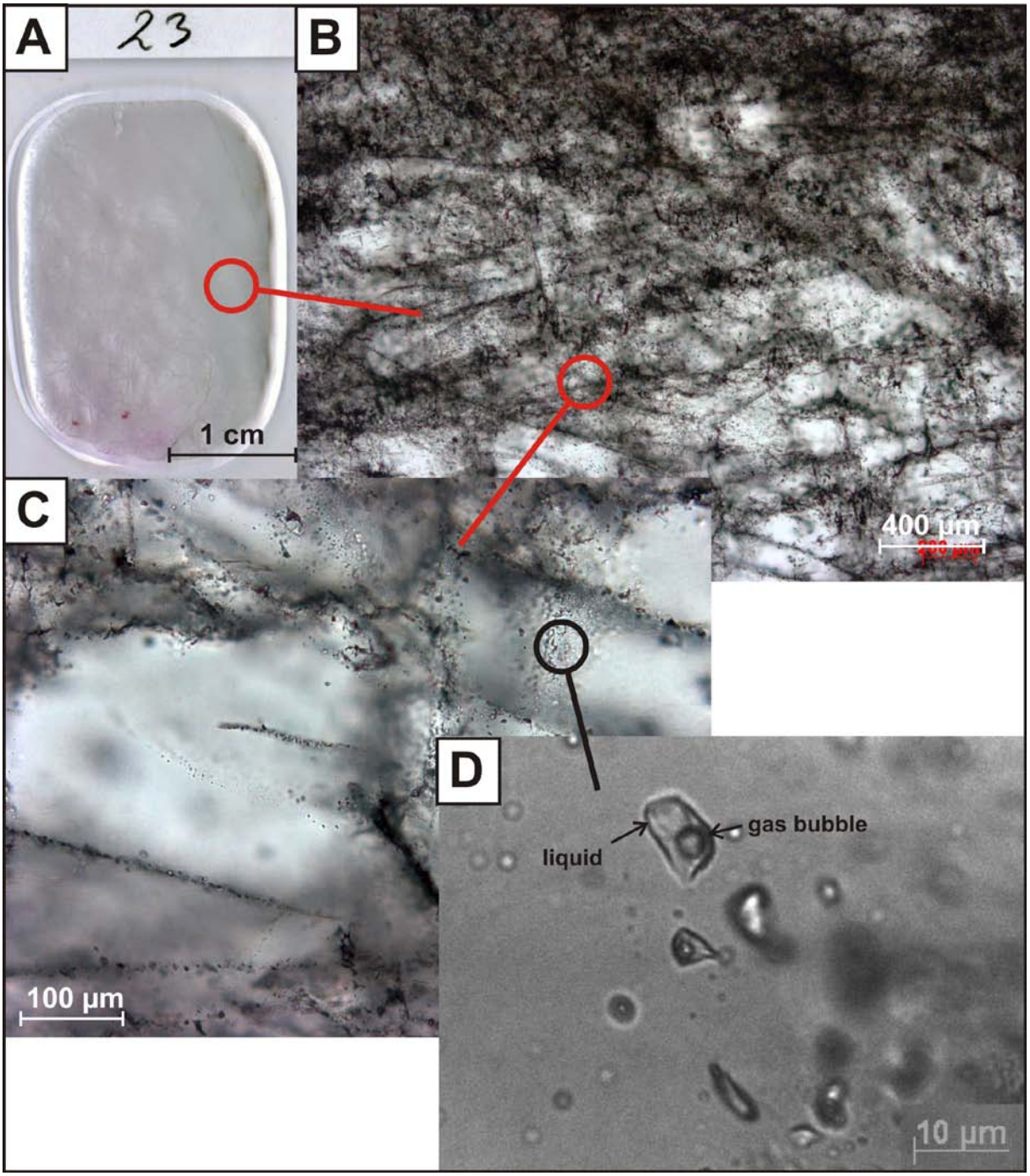

Figure 8. *Microphotographs of quartz sample 23. A – Petrological thick section. B – Optical microscope image (plane light) of quartz showing a high abundance of fluid inclusions causing brownish-black domains (opaqueness) predominantly along healed cracks and grain boundaries. C – Microscopic detail showing clear (fluid inclusion free) domains of quartz and dark trails of fluid inclusions. D – Typical liquid rich fluid inclusions containing gas bubbles.*

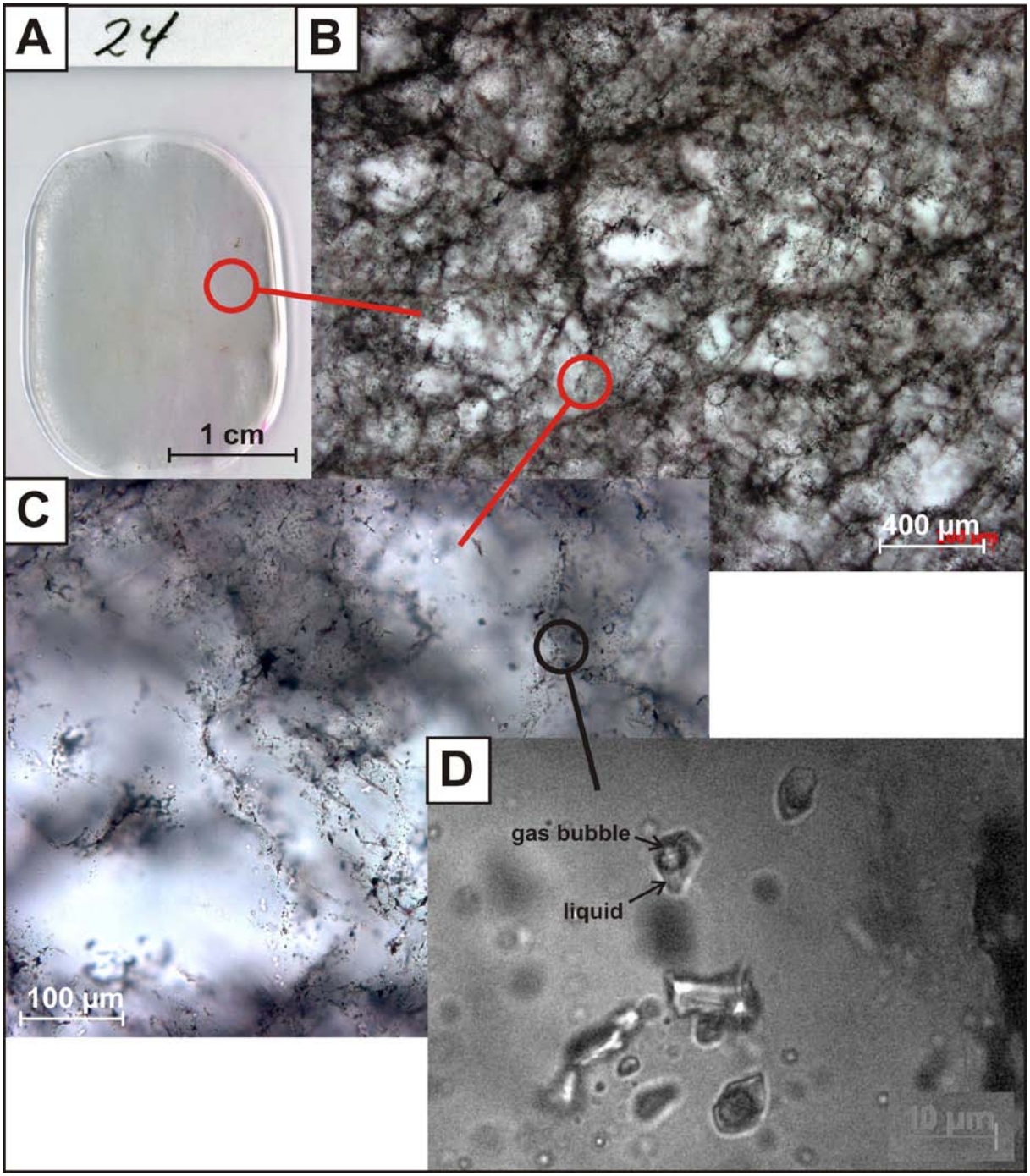

Figure 9. *Microphotographs of quartz sample 24. A – Petrological thick section. B – Optical microscope image (plane light) of quartz showing a high abundance of fluid inclusions causing brownish-black domains (opaqueness). C – Microscopic detail showing clear (fluid inclusion free) domains of quartz and dark trails of fluid inclusions. D – Typical liquid rich fluid inclusions containing gas bubbles.*

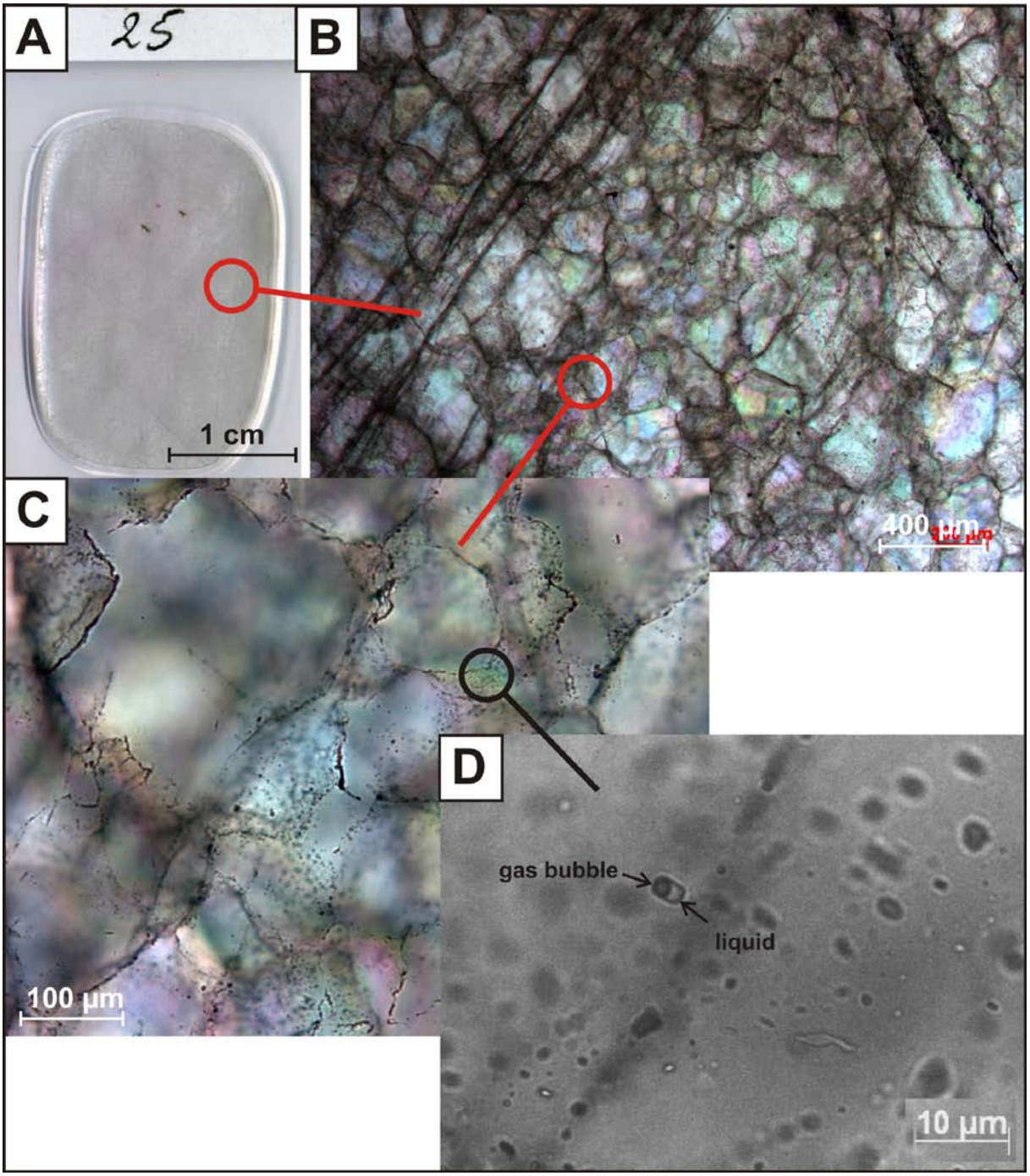

Figure 10. *Microphotographs of quartz sample 25. A – Petrological thick section. B – Optical microscope image (plane light) of quartz showing a high abundance of fluid inclusions causing brownish-black domains (opaqueness) along healed cracks and grain boundaries. C – Microscopic detail showing the mosaic-like texture of quartz texture. The tiny black dots marking the grain boundaries are fluid inclusions. D – Typical liquid rich fluid inclusions containing gas bubbles.*

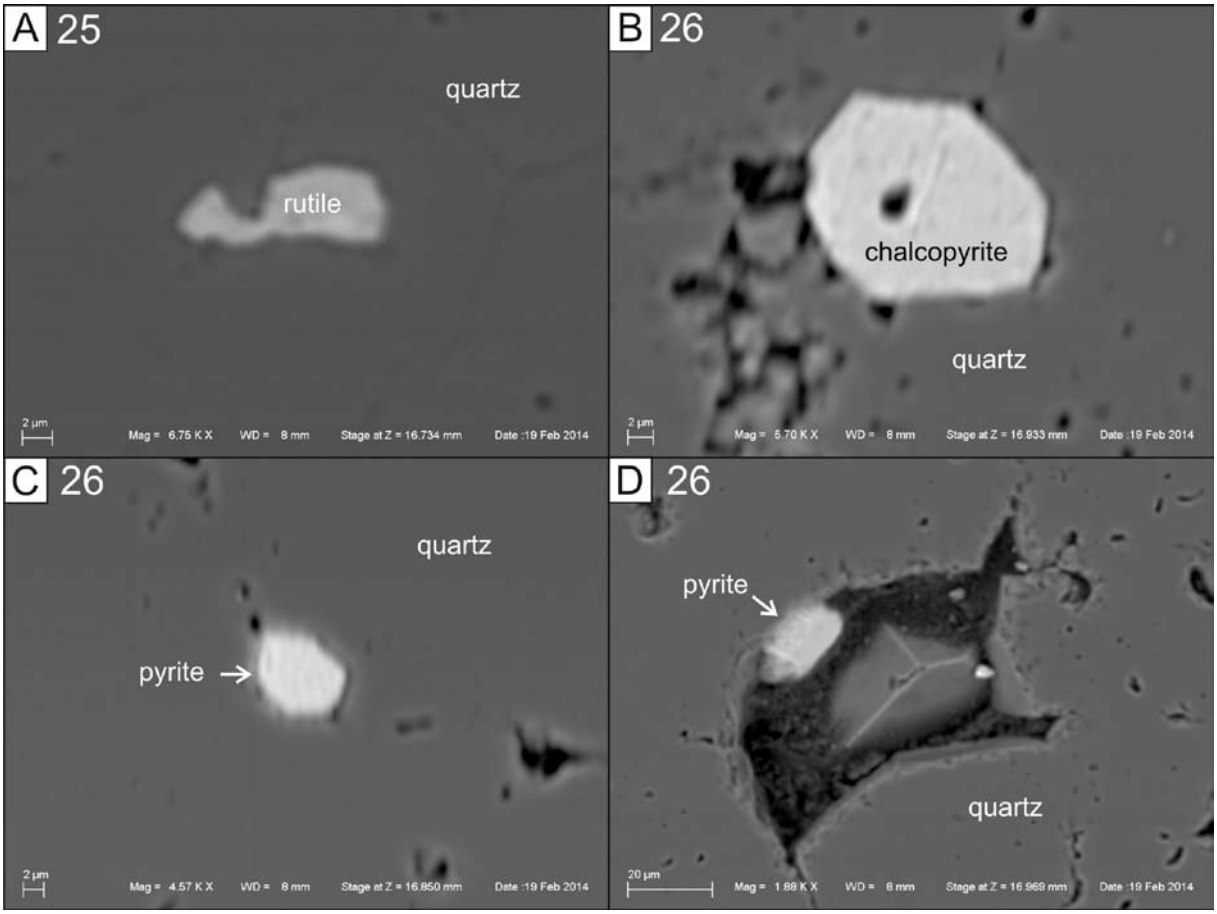

Figure 11. *Backscattered electron images (BSE) of mineral micro inclusions in quartz. A – 8-µm large rutile micro inclusion in sample 25. B – 18-µm large chalcopyrite micro inclusion in sample 26. C – 8-µm large pyrite micro inclusion in sample 26. D – Micro cavity in quartz with a 15-µm large pyrite crystal crystallized at the cavity wall. Sample 26.*

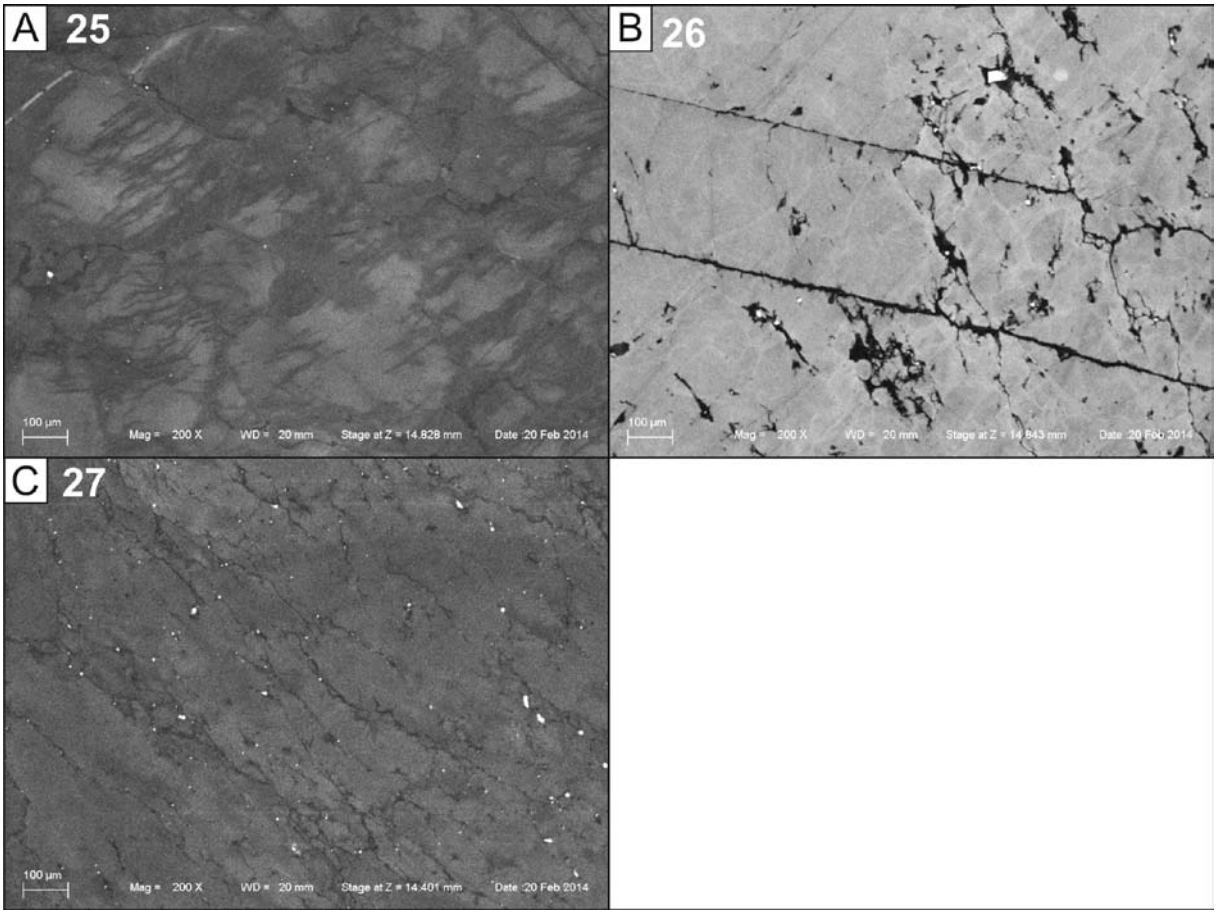

Figure 12. *Scanning electron microscope cathodoluminescence (SEM-CL) images of mineral of quartz. A – Dull luminescent quartz of sample 25. The almost black areas represent domains of newly crystallized quartz to due recrystallization and deformation. The CL features are similar to those of sample 21. B – Bright luminescent quartz of sample 26 superimposed by a secondary non-luminescent (black) generation healing micro fractures and domains around fluid inclusions. C – Dull luminescent quartz of sample 23 with different generations of quartz-healed micro fractures similar to those of samples 22, 23, and 24. The small bright luminescent dots (<1 µm) represent presumably calcite inclusions.*

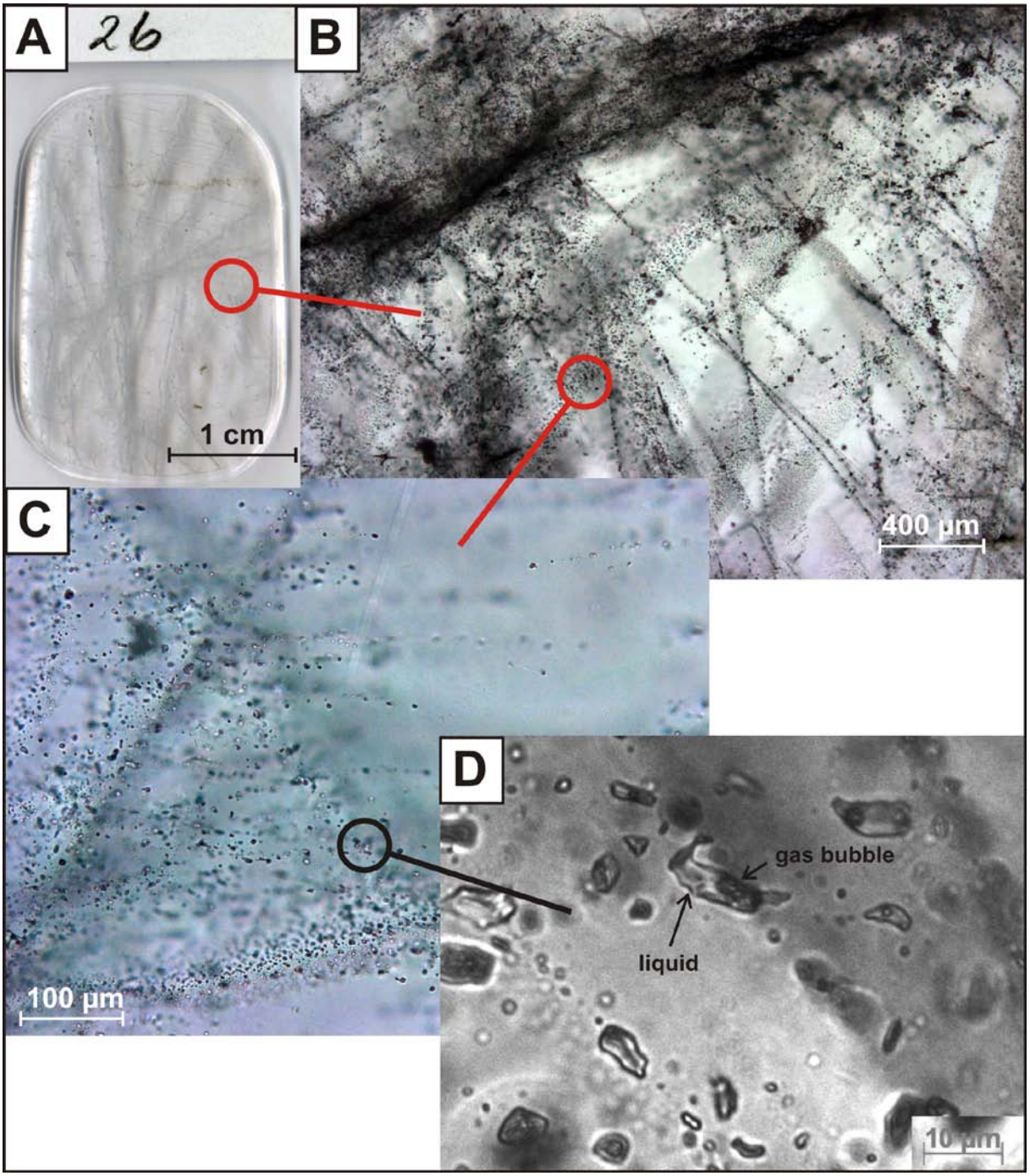

Figure 13. *Microphotographs of quartz sample 26. A – Petrological thick section. B – Optical microscope image (plane light) of a large single quartz showing fluid inclusion trails (black dotted) following healed micro fractures. C – Microscopic detail showing the clear quartz with domains of high fluid inclusion abundance (black dots). D – Typical liquid rich fluid inclusions containing small gas bubbles.*

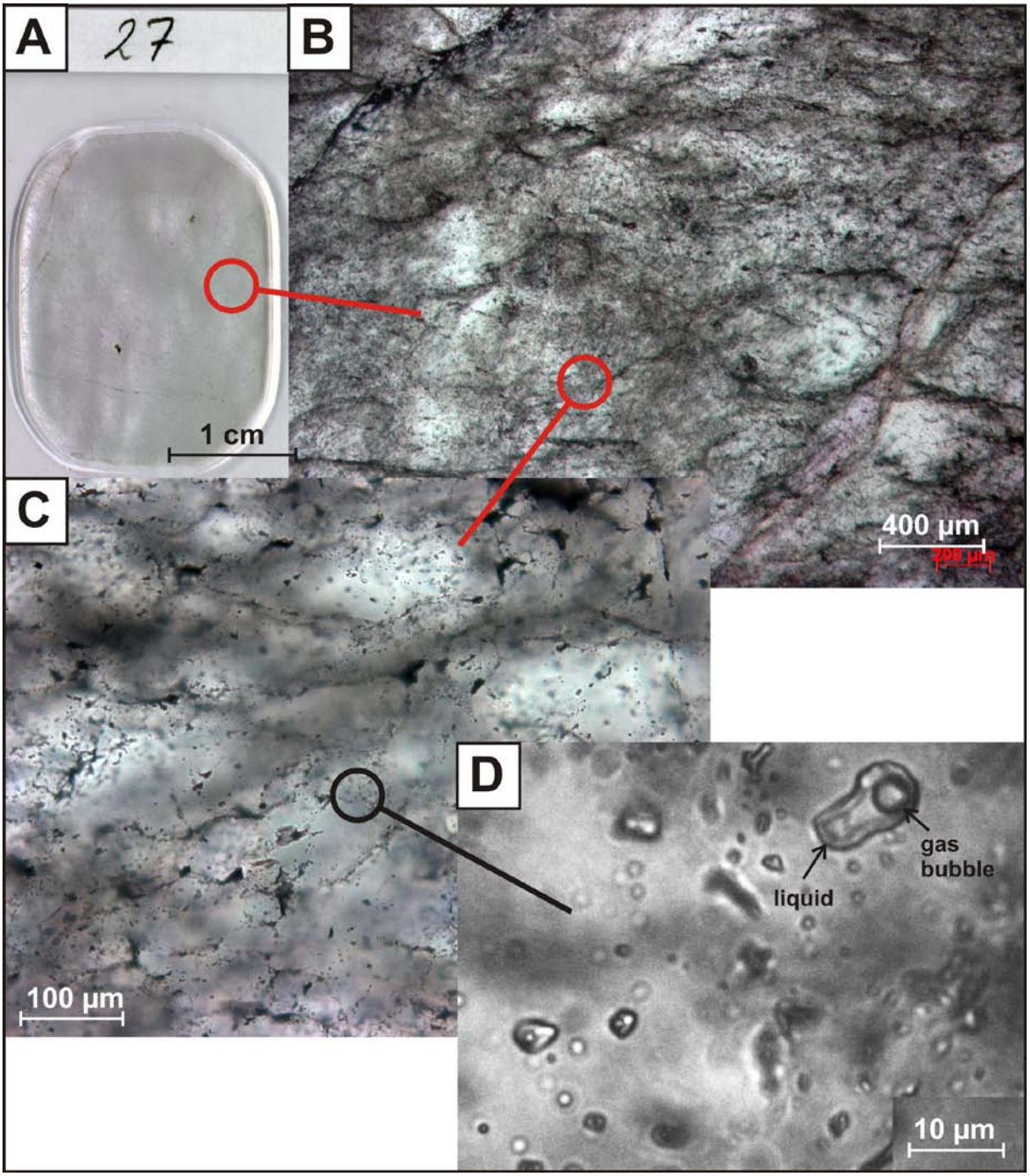

Figure 14. *Microphotographs of quartz sample 27. A – Petrological thick section. B – Optical microscope image (plane light) of quartz showing a high abundance of fluid inclusions causing brownish-black domains (opaqueness). C – Microscopic detail showing the very high abundance of fluid inclusions (black dots/domains). D – Typical liquid rich fluid inclusions containing large gas bubbles.*

3.2 Quartz chemistry

Concentrations of Li, Be, B, Al, P, Ti, Ca, Na, K, Mn, Fe, and Ge were analyzed *in situ* by LA-ICP-MS. The advantage of this method compared to quartz bulk analyses by conventional solution ICP-MS is that the determined concentrations correspond to the contents of ions which are structurally bound in the quartz lattice. Structurally bound trace elements cannot be removed by processing even by hot acid leaching and, thus, they control the chemical quality of the quartz. Thus, the concentrations determined by LA-ICP-MS reflect the best quartz quality which can be achieved by applying the most modern and advanced processing methods available today. However, the quartz grains analyzed in the frame of this project are very rich in fluid inclusions as discussed in the previous chapters and, therefore, concentrations of elements occurring in these fluid inclusions, predominantly Na and K and to some extend Fe and Mn, are superimposed on the concentrations of lattice-bound elements.

3.2.1 Lighthouse & Midway, samples 22, 23, 24, 27

Quartz from the Lighthouse & Midway localities has very low Li (<0.9 ppm) and low Ti (<3.6 ppm; Table 3, Figures 15 and 16). Aluminium concentrations are low to moderately high, varying between 18 and 86 ppm. On the base of the Al content two subgroups of samples can be distinguish: (1) low Al samples 22 and 27 with 18 to 40 ppm Al and (2) moderately high Al samples 23 and 24 with 78 to 110 ppm Al. Sodium and K concentrations higher than the detection limits are caused by fluid micro inclusions which were hit during the ablation process. High Ca is caused by calcite micro inclusions which are relative common in these samples.

3.2.2 Mt. Talbot, samples 21, 25

Quartz from Mt. Talbot has very low Li (<1.0 ppm), low Al (<30 ppm) and generally very low Ti (0.8 to 1.0 ppm; Table 3, Figures 15 and 16). The Ti spike of 4.6 ppm (analysis 25-A) is presumably caused by rutile micro inclusions which were detected in this sample (Figure 11A). Compared to the other two localities the Mt. Talbot quartz has the best and most homogenous chemistry. Concentrations >1 ppm of K and Fe are caused by biotite, magnetite, muscovite and K-feldspar mineral micro inclusions hit during the ablation process (Figures 5A, B, C).

3.2.2 Blow 2, sample 26

Quartz from the locality Blow 2 has high Li (3.3 to 4.2 ppm), Al (130 to 162 ppm), Fe (3.2 to 3.8 ppm), and K (7.1 to 10.8) and very high Ti (19.9 to 20.4 ppm; Table 3, Figures 15 and 16). Because sample 26 contains less fluid inclusions than all other samples the laser ablation raster could be placed in inclusion free area. Thus, the detected high K content represents structurally incorporated K. Talbot quartz has the best and most homogenous chemistry.

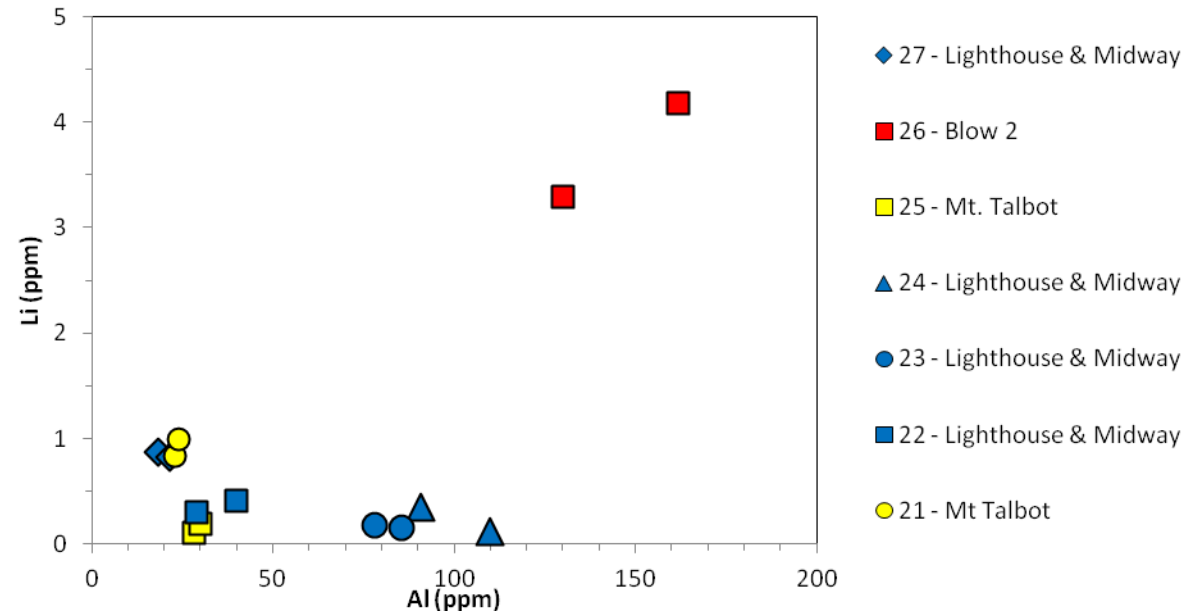

Figure 15. *Graph showing concentrations of Al versus Li in quartz determined by LA-ICP-MS.*

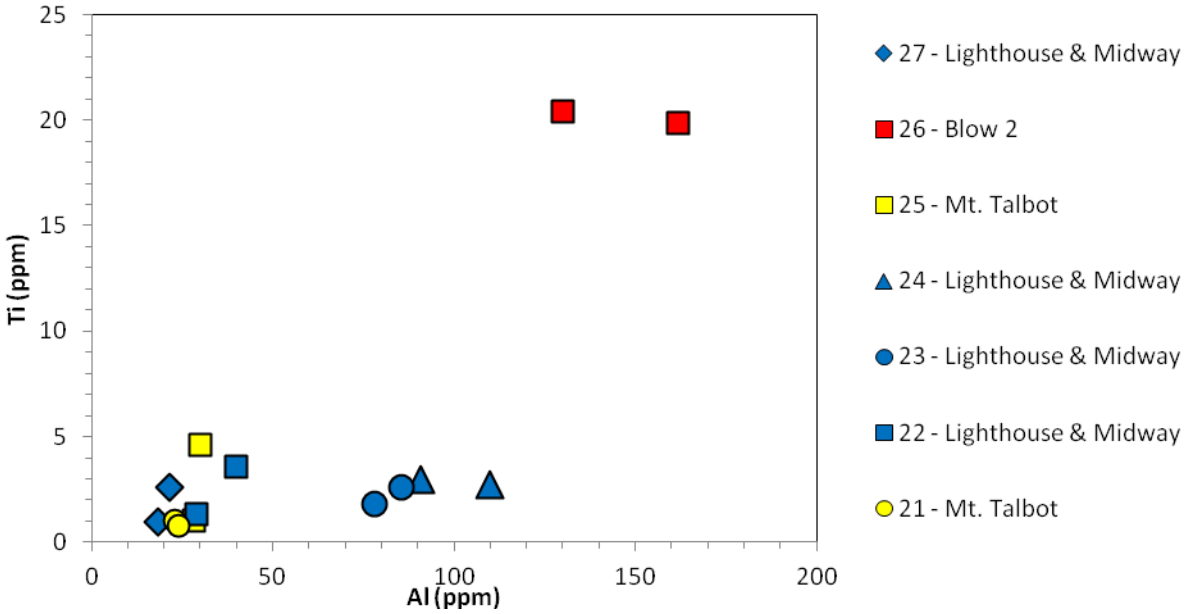

Figure 16. *Graph showing concentrations of Al versus Ti in quartz determined by LA-ICP-MS.*

Table 3. *Concentrations of trace elements (in ppm) of the investigated quartz samples. Two analyses (A and B) were performed on each sample. Elevated concentrations of Na, P, K, Ca, Ti, and Fe, which are superimposed by additional amounts of Na, P, K, Ca, Ti, and Fe from fluid and mineral inclusions are set in parentheses. In the last two rows concentrations of the processed high purity products IOTA STD and IOTA 8 produced by UNIMIN are given for comparison (IOTA 2014). The IOTA 8 quartz sand has the best quality on the market produced from natural quartz. The sum of measured, structural incorporated trace elements (sum) does not consider concentrations of Na, K, and Ca due to the high detection limits and the contamination by fluid inclusions (Na, K) and calcite (Ca). LOD – limit of detection.*

		Li	Be	B	Mn	Ge	Na	Al	P	K	Ca	Ti	Fe	sum
	LOD	0.05	0.02	0.40	0.10	0.16	24.0	3.1	2.9	7.0	5.1	0.97	0.90	
Mt Talbot	21-A	1.00	<0.02	1.51	<0.10	1.06	<24.0	24.2	<2.9	<7.0	<5.1	0.79	(2.90)	34.4
	21-B	0.83	<0.02	1.12	<0.10	0.92	<24.0	22.8	<2.9	<7.0	<5.1	1.01	<0.90	30.6
Lighthouse & Midway	22-A	0.41	<0.02	1.81	<0.10	1.15	(60.5)	39.7	<2.9	<7.0	(7.9)	3.55	(2.71)	52.4
	22-B	0.30	0.07	1.84	<0.10	0.75	(173.6)	29.1	<2.9	<7.0	(6.9)	1.34	(2.13)	38.5
Lighthouse & Midway	23-A	0.18	<0.02	1.34	<0.10	0.74	<24.0	78.0	(6.4)	(8.7)	<5.1	1.79	<0.90	89.5
	23-B	0.16	<0.02	1.13	0.15	0.51	<24.0	85.6	<2.9	(26.1)	<5.1	2.58	<0.90	93.9
Lighthouse & Midway	24-A	0.35	<0.02	0.69	0.34	0.99	<24.0	90.8	<2.9	(28.2)	(8.2)	2.95	(2.94)	102.0
	24-B	0.12	<0.02	1.77	0.49	0.89	(67.2)	110.0	<2.9	(114.0)	(62.6)	2.75	(7.71)	126.7
Mt Talbot	25-A	0.19	<0.02	1.01	0.47	0.87	<24.0	29.9	<2.9	(115.2)	<5.1	(4.61)	(17.66)	57.6
	25-B	0.10	<0.02	1.20	0.22	0.75	<24.0	28.3	<2.9	<7.0	<5.1	1.01	(2.76)	37.3
Blow 2	26-A	4.17	0.25	1.06	0.85	1.38	<24.0	161.9	<2.9	10.8	<5.1	19.88	3.76	196.2
	26-B	3.29	0.28	0.94	0.71	1.07	<24.0	130.1	<2.9	7.4	<5.1	20.38	3.20	162.9
Lighthouse & Midway	27-A	0.82	<0.02	1.65	0.80	0.50	<24.0	21.4	<2.9	(43.3)	(5.3)	2.60	<0.90	31.6
	27-B	0.87	<0.02	1.99	0.67	0.88	<24.0	18.4	<2.9	<7.0	<5.1	0.95	<0.90	27.6
IOTA STD		0.5	-	<0.10	0.04	-	1.0	14.0	0.1	0.6	0.5	1.2	0.3	16.2
IOTA 8		<0.05	-	<0.05	0.001	-	<0.05	8.0	<0.05	<0.05	0.4	1.3	<0.05	9.5

4. Summary and discussion

The micro inclusion inventory of quartz samples was examined by optical and scanning electron microscopy. Concentrations of structurally bound (lattice-bound) trace elements were analyzed by LA-ICP-MS. Because lattice-bound trace elements cannot be removed by processing, these concentrations correspond to the lowest concentrations (best chemical quality) which may be achieved if the most modern and advanced quartz processing techniques are applied including floatation, magnetic separation, and acid leaching of ground quartz sand (e.g. Haus 2005). It is important to note that the trace element concentrations determined by LA-ICP-MS will not correspond to the trace element concentrations of an unprocessed quartz product. However, quartz grains analyzed in the frame of this project are very rich in fluid micro inclusions (0.1 to 40 µm) and contain commonly mineral micro inclusions (5 to 400 µm) and, therefore, concentrations of elements occurring in these inclusions, predominantly Na, K, Ca, and Fe, come in addition to the concentrations of lattice-bound elements.

The trace element content and type and frequency of micro fluid and mineral inclusions in quartz are characteristically for the three different investigated deposit areas and are as follows:

Quartz from *Mt. Talbot* (samples 21, 25) has a distinctive inventory of mineral micro inclusions including muscovite ($KAl_2(AlSi_3O_{10})(OH)_2$), K-feldspar ($(K,Na)AlSi_3O_8$), biotite, ($K(Fe,Mg)Al(Al_2Si_2O_{10})(OH)_2$), rutile ($TiO_2$), and magnetite ($Fe_2O_3$). In addition, liquid-rich fluid inclusions are very common giving the quartz the milky and opaque appearance. The properties of the fluid inclusions indicate a moderate salinity of the fluid with 3 to 8 vol.% NaCl(+KCl)making them significant Na and K contaminants. The fluid and mineral inclusions sit predominantly at boundaries of micro-crystalline grains. The grains have an average size of 250 µm. The central parts of the grains are almost free of mineral and fluid inclusions. The Mt. Talbot quartz has the lowest total trace element contents of 38 to 58 ppm, without considering Ca, Na, and K due to their high detection limits. The concentrations of the analyzed elements are generally below the suggested maximum values of the high-purity quality requirements. High-purity quartz (HPQ) is defined as quartz containing less than 50 ppm (= 99.995 % SiO_2) of contaminating elements (Harben 2002, Müller et al. 2012). The upper concentration limits for the individual trace elements in high purity quartz are suggested as follows: Al <30 ppm, Ti <10 ppm, Li <5 ppm, K <8 ppm, Na <8 ppm, Ca <5 ppm, P <2 ppm, Fe <3 ppm, and B <1 ppm (Müller et al. 2012). The high K, Ti, and Fe concentrations of analysis 25-A are caused by micro inclusions of biotite (K, Fe) and rutile (Ti). Thus, these high concentrations are not caused by structurally bound trace elements and can possibly be removed by advanced processing. Structurally incorporated (lattice-bound) trace elements cannot be removed by processing. Quartz crushing and grinding down to grain sizes of about 500 µm followed by acid leaching will possibly be able to remove most of the mineral and fluid micro inclusions. The product will be highly suitable for solar-grade silicon production. By applying advanced processing technology, the quartz can possibly be used for optical glass production.

Quartz from *Lighthouse & Midway* (samples 22, 23, 24, 27) is strongly recrystallized and very rich in fluid inclusions. The latter are responsible for the milky and opaque appearance of the quartz. They occur within crystals, along healed micro fractures and along grain boundaries. The inclusions contain fluids with high salinities between 5 and 15 wt% NaCl(+KCl) and are therefore significant Na and K contaminants. The removal of product-contaminating fluid inclusions occurring within crystals (intra-crystalline) requires thermal

treatment and calcination (Haus 2005). In addition, the occurrence of calcite ($CaCO_3$) micro inclusions is a characteristic feature of the Lighthouse & Midway quartz. Quartz from Lighthouse & Midway has variable total trace element concentrations between 28 and 127 ppm without considering Ca, Na, and K due to the high detection limits. On the base of the Al content two subgroups of samples can be distinguish: (1) low Al samples 22 and 27 with 18 to 40 ppm Al and (2) moderate high Al samples 23 and 24 with 78 to 110 ppm Al. Na and K concentrations higher than the detection limits are caused by fluid inclusions which were hit during the ablation process. High Ca is caused by calcite micro inclusions which might be removed by acid leaching of crushed and ground quartz sand. Due to the variable and partially moderately high content of structurally incorporated Al and the high abundance of intra-crystalline fluid inclusions, a possible processed quartz product will ideally fulfil the requirements for intermediary quality (Harben 2002, Müller et al. 2012). However, the quality of simple processed quartz will possibly be sufficient to use it as raw material for solar-grade silicon production due to relatively low B and P concentrations.

The megacrystic quartz from *Blow 2* (sample 26) shows a high abundance of fluid inclusions but they are less common compared to the other investigated quartz samples. The inclusions occur along trans-granular trails following healed micro fractures. The properties of the fluid inclusions indicate a moderate salinity of the fluid with 3-8 vol.% NaCl(+KCl) and the inclusions are therefore significant Na and K contaminants. The removal of these product-contaminating inclusions requires thermal treatment and calcination (Haus 2005). Pyrite (FeS_2) and chalcopyrite ($CuFeS_2$) micro inclusions are characteristically for the Blow 2 sample. They represent significant Fe contaminants. It will be challenging to remove the Fe sulfide inclusions by processing because they occur within quartz crystals. Quartz from Blow 2 has high Li, Al, Fe, and K and very high Ti. The total content of the analysed structurally incorporated trace elements is 163 and 196 ppm without considering Ca, Na, and K due to the high detection limits. On the base of the moderate high total trace element content a possible processed quartz product will ideally fulfil the requirements of intermediary quality (Harben 2002, Müller et al. 2012). The data imply that the quartz from this deposit cannot serve as raw material for optical glass production due to its high Ti content. However, simple processed quartz may be fulfil the quality requirements of solar-grade silicon production due to relative low B and P concentrations.

This report represents an evaluation of the chemical quality potential of the investigated samples. In order to achieve the described maximum (best) quality of the final quartz product, most of the fluid inclusions and non-quartz mineral inclusions and coatings described here have to be removed by advanced processing including crushing, flotation, magnetic and electrostatic separation, and possibly acid leaching, thermal treatment and calcination (e.g., Haus 2005). However, advice for the performance of the quartz processing is outside the competence of the Geological Survey of Norway and, therefore, other institutions or companies should be consulted.

5. References

Flem B., Müller A. (2012) In situ analysis of trace elements in quartz using laser ablation inductively coupled plasma mass spectrometry. In: Götze J., Möckel R. (eds.) Quartz: Deposits, mineralogy and analytics. Springer Geology, Berlin, Heidelberg, p. 219-236. DOI: 10.1007/978-3-642-22161-3_10

Flem B., Larsen R.B., Grimstvedt A., Mansfeld J. (2002) In situ analysis of trace elements in quartz by using laser ablation inductively coupled plasma mass spectrometry. Chemical Geology 182: 237–247.

GeoReM (2011) Geological and environmental reference materials. <http://georem.mpchmainz> gwdg.de. Accessed 2 Feb 2014.

Götze J., Plötze M., Habermann D. (2001) Origin, spectral characteristics and practical applications of the cathodoluminescence (CL) of quartz—a review. Mineralogy and Petrology 71: 225–250.

Harben P.W. (2002) The industrial mineral handybook—a guide to markets, specifications and prices. 4th edn. Industrial Mineral Information, Worcester Park, p 412

IOTA 2014. IOTA Quartz. <http://www.iotaquartz.com/product-range.cfm> Accessed March 5 2014.

Haus R. (2005) High demands on high purity – processing high purity quartz and diatomite. Industrial Mineral 42: 62-67 (October).

Müller A., Lennox P., Trzebski R. (2002) Cathodoluminescence and micro structural evidence for crystallisation and deformation processes in quartz of S- and I-type granites in the Eastern Lachlan Fold Belt (SE Australia). Contributions to Mineralogy and Petrology 143: 510-524

Müller A., Wiedenbeck M., Flem B., Schiellerup H. (2008) Refinement of phosphorus determination in quartz by LA-ICP-MS through defining new reference material values. Geostandards and Geoanalytical Resarch 32: 361–376.

Müller A., Wanvik J. E., Ihlen P.M. (2012) Petrological and chemical characterisation of high-purity quartz deposits with examples from Norway. In: Götze J., Möckel R. (eds.) Quartz: Deposits, mineralogy and analytics. Springer Geology, Berlin, Heidelberg, p. 71-118. DOI: 10.1007/978-3-642-22161-3_4.

Norges geologiske undersøkelse
Postboks 6315, Sluppen
7491 Trondheim, Norge

Besøksadresse
Leiv Eirikssons vei 39, 7040 Trondheim

Telefon 73 90 40 00
Telefax 73 92 16 20
E-post ngu@ngu.no
Nettside www.ngu.no

Geological Survey of Norway
PO Box 6315, Sluppen
7491 Trondheim, Norway

Visitor address
Leiv Eirikssons vei 39, 7040 Trondheim

Tel (+ 47) 73 90 40 00
Fax (+ 47) 73 92 16 20
E-mail ngu@ngu.no
Web www.ngu.no/en-gb/